**Crystal structures and magnetic properties of dimorphic $Li_3OsO_4$**

Hai L. Feng,[1#*] Manfred Reehuis,[2] Andreas Hoser,[2] Martin Valldor,[1,3] Martin Jansen[1,4*]

[1]Max Planck Institute for Chemical Physics of Solids, D-01187 Dresden, Germany

[2]Helmholtz-Zentrum Berlin für Materialien und Energie, D-14109 Berlin, Germany

[3]Leibniz Institute for Solid State Research (IFW), D-01069 Dresden, Germany

[4]Max Planck Institute for Solid State Research, D-70569 Stuttgart, Germany

Corresponding authors:
hai.feng_nims@hotmail.com (HLF)
m.jansen@fkf.mpg.de (MJ)

#Current address: Department of Chemistry and Chemical Biology, Rutgers, the State University of New Jersey, Piscataway, NJ 08854, USA

**Abstract:** Rocksalt-type oxides $Li_3OsO_4$ with disordered and ordered arrangements of Li and Os were synthesized. The disordered phase crystallizes in the ideal rocksalt structure with cubic space group $Fm\bar{3}m$, while the ordered polymorph adopts the monoclinic $Na_3BiO_4$-type structure (space group *P*2/*c*). The analyses of X-ray and neutron diffraction data of monoclinic $Li_3OsO_4$ indicate that there is a considerable anti-site disorder of Li and Os and that the sample is nonstoichiometric ($Li_{3.045(5)}Os_{0.955(5)}O_4$). In monoclinic $Li_3OsO_4$ the $OsO_6$ octahedra are not isolated from each other but they form edge-sharing zigzag chains. Both cubic and monoclinic $Li_3OsO_4$ are electrically semiconducting. Cubic $Li_3OsO_4$ does not show any sign of magnetic order down to 2 K, whereas the $\chi(T)$ data of monoclinic $Li_3OsO_4$ display an anomaly at 310 K. However, the neutron diffraction study indicated no evidence of long-range magnetic order. The anomaly at 310 K may be caused by short-range antiferromagnetic ordering within the individual Os chains.

**Keywords:** $Li_3OsO_4$; Rocksalt; $Na_3BiO_4$; zigzag chain; antiferromagnetic.

## 1. Introduction

Rocksalt-type oxides have come into focus as functional materials and have been extensively studied since the 1980s, after the historical finding of $LiCoO_2$ being a high performance cathode material [1]. Many further lithium oxides with rocksalt structure, such as $LiVO_2$, $LiNiO_2$, $Li_2MnO_3$, $Li_2TiO_3$, and $Li_3NbO_4$-based materials, have been reported as possible cathode materials [2–8]. Some rocksalt-type oxides display polymorphism featuring ordered or disordered arrangements of cations [9–11]. Ordered rocksalt type transition metal oxides can form lattices which are of interest for their magnetic states. A spin-liquid magnetic ground state has been proposed for $LiNiO_2$ and $NaTiO_2$ [12–14]. $Na_3Cu_2SbO_6$ was reported to have a singlet ground state [15], while isostructural $Na_3Co_2SbO_6$ shows long-range antiferromagnetic ordering [16].

Compared with 3*d* transition metals, the 4*d*/5*d* representatives in general show larger spin-orbit couplings, weaker Coulomb repulsion, and larger crystal field splitting energy, which results in particular interplays between charge, spin, and orbital degrees of freedom [17]. For instance, hyper-honeycomb iridate β-$Li_2IrO_3$ has been considered a platform for Kitaev magnetism [18–20]. Rocksalt-type osmates such as $Li_4MgOsO_6$ ($Os^{6+}$), and $Li_5OsO_6$ ($Os^{7+}$) with long-range magnetic order or magnetic frustration have been reported [21,22]. From a chemistry point of view, osmium is capable of adopting a wide range of oxidation states from –2 to +8. Oxides containing $Os^{5+}$ are of particular interest, for example $NaOsO_3$ shows a metal-insulator transition and metallic $LiOsO_3$ display a ferroelectric-like structural transition [23–25]. In this work, we targeted a rocksalt-type osmate with $Os^{5+}$. We synthesized $Li_3OsO_4$ with both ordered and disordered arrangement of Li and Os. While the crystal structure of disordered cubic $Li_3OsO_4$ was reported earlier [26], here the cation ordered monoclinic phase has been obtained for the first time.

## 2. Experimental

Cubic $Li_3OsO_4$ was synthesized by solid state reactions of $Li_2O$, $OsO_2$, and $KClO_4$ under the pressure of 2 GPa. $Li_2O$ was prepared by thermal decomposition of LiOH (Alfa Aesar, 98 %) according to Brauer [27]. About 80 mg of $Li_2O$, $OsO_2$, and $KClO_4$ in a molar ratio of $^3/_2$ : 1 : $^1/_8$ were well ground together in an Ar-filled glovebox and then sealed in a gold capsule (diameter of 1.5 mm; length of 5.0 mm). The gold crucible was compressed in a piston cylinder press at a pressure of 2 GPa, and was heated at 800 °C for 1 hour. After quenching to ambient temperature the pressure was released.

Monoclinic $Li_3OsO_4$ was synthesized by solid state reactions of $Li_2O$, $Li_2O_2$ (95%, Alfa), and $OsO_2$ (Os 83%, alfa) in a molar ratio 1 : ½ : 1. About 400 mg of constituents were mixed together and pressed into a pellet inside an Ar-filled glovebox, and then the pellet was loaded into a corundum crucible inside a silica tube (diameter of 8 mm). The silica tube was then sealed under dynamic vacuum using a $H_2/O_2$ torch, and heated at 750°C for 48 hours in a tube furnace. Note that the length of the sealed silica ampule is about 150 mm. Along with this procedure, about 3 grams of $Li_3OsO_4$ were synthesized for neutron powder diffraction.

Both synthesized samples are black. Small pieces of each $Li_3OsO_4$ samples were cut from the synthesized pellets and finely ground to collect X-ray diffraction (XRD) patterns (Guinier technique, Huber G670 camera, Cu-Kα1 radiation, $\lambda$ = 1.54056 Å, germanium monochromator, $10^o \leq 2\theta \leq 85^o$, the step width of 0.005º). The refinement of crystal structures was carried out by Rietveld analysis using the RIETAN-VENUS program [28], and the crystal structure was drawn using the VESTA software [29].

The neutron powder diffraction experiments were carried out on the instruments E2

and E6 at the BER II reactor of the Helmholtz-Zentrum Berlin, where powder patterns were recorded in the ranges of $2\theta$ = 7.8 and 83.4 ° (E2) and $2\theta$ = 5.5 and 136.5 ° (E6), respectively. Both instruments use a pyrolytic graphite (PG) monochromator to select the neutron wavelength $\lambda$ = 2.38 Å (E2) and $\lambda$ = 2.43 Å (E6), respectively. The powder sample of monoclinic $Li_3OsO_4$ was filled in a vanadium container with the dimensions $d$ = 6 mm and $h$ = 40 mm. The temperature dependence of the structural properties was investigated on E6 between 2 and 353 K using an Orange Cryofurnace (AS Scientific Products Ltd., Abingdon, GB). In order to follow in detail the structural changes, we collected 30 powder patterns in this temperature range. Rietveld refinements of the powder diffraction data were carried out with the program *FullProf* [30], using the nuclear scattering lengths $b$(Li) = –1.90 fm, $b$(O) = 5.805 fm, $b$(Os) = 11.0 fm [31]. In order to achieve a detailed magnetic structure analysis, neutron powder diffraction patterns were collected at $T$ = 2 and 298 K on the instrument E2 with high counting statistics (24 h/pattern) using a 15-min collimation to improve the instrumental resolution.

Using pieces of the obtained pellet, the electrical resistivity ($\rho$) was measured with a DC gauge current of 0.1 mA by the four-point method using a physical properties measurement system (PPMS, Quantum Design, Inc.). Electrical contacts were made with Pt wires and silver glue. The magnetic susceptibilities ($\chi$) of the samples were measured in a SQUID magnetometer (MPMS, Quantum Design), at zero-field cooled (ZFC) and field cooling (FC) conditions in the temperature range of 2 to 380 K under applied magnetic fields of 10 kOe.

## 3. Results and discussions

**Crystal structures**. The XRD pattern of the sample synthesized at 2 GPa and 800 °C,

shown in Fig. 1, can be well Rietveld refined assuming the cubic structure with space group $Fm\overline{3}m$, which is consistent with the cubic $Li_3OsO_4$ reported [26]. This space group has been shown to be adapted by similar oxides like $Li_3MoO_4$, $Li_3NbO_4$, and $Li_3TaO_4$ [10,32,33]. In cubic $Li_3OsO_4$, the 4*a* site is shared by Li and Os atoms, and the 4*b* site is occupied by O atoms. Besides the main phase $Li_3OsO_4$, the XRD pattern indicates presence of 1.5%wt of KCl, which stems from $KClO_4$ used as an oxygen source, and further 0.8%wt of Os metal is noticeable. It is should be noted that calculated weight percent for KCl from starting materials ($Li_2O$, Os, and $KClO_4$) is 1.25%wt. The results of the Rietveld refinements for cubic $Li_3OsO_4$ are summarized in Table 1.

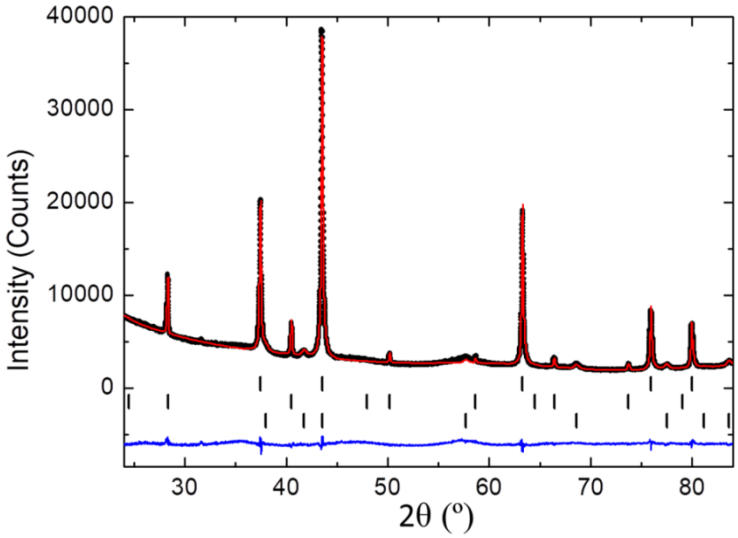


Fig. 1. Rietveld refinement of the powder XRD pattern of cubic $Li_3OsO_4$. The calculated patterns (red) are compared with the observed ones (black circles). The difference of patterns is shown as a blue curve. Black vertical bars indicate the Bragg reflection positions for the cubic $Li_3OsO_4$ (top), KCl (middle), and Os (bottom).

The XRD pattern (see Fig. 2a) of the sample synthesized at 750 °C under ambient pressure can be well refined assuming the $Na_3BiO_4$ type structure (space group *P*2/*c*) [34], which was originally determined using single-crystal data and reported to apply for similar oxides $Li_3SbO_4$, and $Li_3RuO_4$ [35,36,37]. In this structure, there are four

distinguishable sites for cations, where Li1/Os1 and Li2/Os2 are located at the Wyckoff position 2*e* (0,*y*,¼) and Li3/Os3 and Li4/Os4 at 2*f* (½,*y*,¼), respectively. The refinements indicated that the Li1/Os1 site is dominantly occupied by Os, whereas the other sites are Li dominant sites (see Fig. 3). The Rietveld refinements suggested a small amount of Os deficiency and resulted in a nonstoichiometric composition of $Li_{3.056(2)}Os_{0.944(2)}O_4$.

Because of the weak X-ray scattering power of Li, it is difficult to accurately determine its position, especially in the presence of a strong scatterer Os. Therefore we complementarily used the neutron-diffraction technique to reveal in detail the structural properties of $Li_3OsO_4$. Rietveld refinements of the data set collected at the highest temperature of 353 K (see Fig. 2b) converged to a satisfactory residual $R_F$ = 0.0233 (defined as $R_F = \sum||F_{obs}| - |F_{calc}||/\sum|F_{obs}|$), confirming the $Na_3BiO_4$-type structure with the space group *P*2/*c*. These results are in full agreement with the results of our XRD study. The sample contained 0.66(3) % of $Li_2CO_3$ which was taken into account in the Rietveld refinement. The $Li_2CO_3$ may be resulted by the reaction of $Li_2O$ and $CO_2$ in air. Here the structural parameters of $Li_2CO_3$, given in Ref. 38, were used. It was found that the site Li1/Os1 in $Li_3OsO_4$ is mainly occupied with Os, while the other three sites mainly contain Li. Here it has to be mentioned that the standard deviations of the positional parameters *y*(Li2/Os2) and *y*(Li3/Os3) are considerably enlarged (Table 1). This can be ascribed to the fact that neutron scattering length of Li is negative [*b*(Li) = −1.90 fm] and much smaller than [*b*(Os) = +11.0 fm] which completely compensate each other at a critical concentration of 85% Li. The Li concentration at the Li2/Os2 site lies nearest to this critical value and therefore the sigma of *y*(Li2/Os2) is the largest.

The refinements also indicate that both oxygen sites 4*g* (*x*,*y*,*z*), O1 and O2 are fully occupied. The refinement results of the neutron data also indicate a small amount of Os

deficiency and give a nonstoichiometric composition of $Li_{3.045(5)}Os_{0.955(5)}O_4$, which is close to the composition obtained from X-ray analysis. We presume the formation of volatile $OsO_4$ during the synthesis to be responsible for the Os deficiency. The results of the Rietveld refinements for both, X-ray and neutron diffraction data, are summarized in Table 1. Compared to monoclinic $Li_3RuO_4$, in which Ru-dominant site is fully occupied by Ru and the Li-dominant sites are partially occupied by Ru with 1.0% - 1.7% [37]. The monoclinic $Li_{3.045(5)}Os_{0.955(5)}O_4$ show much higher degree of anti-site disorder between Li and Os site: 17.1% of Os-dominant Li1/Os1-site was occupied by Li and Li-dominant Li2/Os2, Li3/Os3, and Li4/Os4-sites partially occupied by Os with 0.6% - 9.8% (see Table 2).

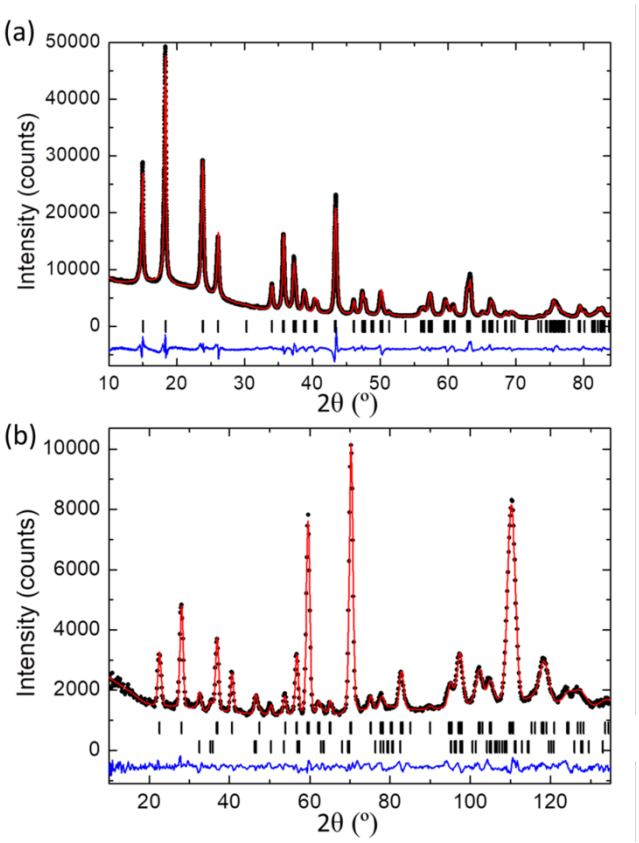


Fig. 2. X-ray (at 299 K) and neutron powder diffraction patterns (at 353 K, instrument E6) of monoclinic $Li_3OsO_4$. The calculated patterns (red) are compared with the observed ones (black circles). The difference of patterns is shown as a blue curve. Black

vertical bars indicate the Bragg reflection positions for title phase and impurity phase $Li_2CO_3$, respectively. (For interpretation of the references to colour in this figure legend, the reader is referred to the Web version of this article).

Table 1. Results of the X-ray and neutron diffraction studies of cubic and monoclinic $Li_3OsO_4$. Listed are the unit cell and positional parameters as well as the refined occupancies at the Li/Os sites.

| Atom | Site | *x* | *y* | *z* | *occ* | $B_{iso}$ (Å$^2$) |
|---|---|---|---|---|---|---|
| Cubic $Li_3OsO_4$ at 299 K (X-ray diffraction). Space group $Fm\bar{3}m$: $a$ = 4.1551(2) Å, $V$ = 71.738(5) Å$^3$, $Z$ = 1, $R_{wp}$ = 3.58%, $R_P$ = 2.75%, $\chi^2$ = 2.189. | | | | | | |
| Li/Os | 4a | 0 | 0 | 0 | 0.75/0.25 | 1.28(2) |
| O | 4b | 0.5 | 0.5 | 0.5 | 1 | 1.28(2) |
| Monoclinic $Li_3OsO_4$ at 299 K (X-ray diffraction). Space group $P2/c$: $a$ = 5.1154(6) Å, $b$ = 5.8845(7) Å, $c$ = 5.0679(5) Å, $\beta$ = 109.686(3) °, $V$ = 143.64(3) Å$^3$, $Z$ = 2, $R_{wp}$ = 4.67%, $R_P$ = 3.62%, $\chi^2$ = 4.04. | | | | | | |
| Li1/Os1 | 2*e* | 0 | 0.1316(6) | 0.25 | 0.149(4) /0.851 | 0.45(2) |
| Li2/Os2 | 2*e* | 0 | 0.628(4) | 0.25 | 0.925(1)/0.075 | 0.45(2) |
| Li3/Os3 | 2*f* | 0.5 | 0.126(11) | 0.75 | 0.997(1)/0.003 | 0.45(2) |
| Li4/Os4 | 2*f* | 0.5 | 0.392(7) | 0.25 | 0.986(1)/0.014 | 0.45(2) |
| O1 | 4*g* | 0.2034(11) | 0.1096(16) | 0.0058(17) | 1 | 0.45(2) |
| O2 | 4*g* | 0.7760(11) | 0.3518(16) | 0.0089(16) | 1 | 0.45(2) |
| Monoclinic $Li_3OsO_4$ at 353 K (neutron diffraction). Space group $P2/c$: $a$ = 5.1062(11) Å, $b$ = 5.8903(11) Å, $c$ = 5.0805(10) Å, $\beta$ = 109.75(2) °, $V$ = 143.82(9) Å$^3$, $Z$ = 2, $R_F$ = 0.0233. | | | | | | |
| Li1/Os1 | 2*e* | 0 | 0.131(4) | 0.25 | 0.171(5)/0.829 | 0.86(8) |
| Li2/Os2 | 2*e* | 0 | 0.65(3) | 0.25 | 0.902(5)/0.098 | 0.86(8) |
| Li3/Os3 | 2*f* | 0.5 | 0.121(20) | 0.75 | 0.978(5)/0.022 | 0.86(8) |
| Li4/Os4 | 2*f* | 0.5 | 0.440(8) | 0.25 | 0.994(6)/0.006 | 0.86(8) |
| O1 | 4*g* | 0.2249(18) | 0.1183(15) | 0.0062(26) | 1 | 0.86(8) |
| O2 | 4*g* | 0.7589(16) | 0.3509(17) | 0.0055(22) | 1 | 0.86(8) |

Table 2. Selected bond lengths and angels of monoclinic $Li_3OsO_4$ (neutron diffraction at 353 K).

| Bond length | (Å) | Bond angle | (º) |
|---|---|---|---|
| Li1/Os1–O1 | 1.954(8) × 2 | O1–Li1/Os1–O1 | 175.6(3) |
| Li1/Os1–O1 | 2.04(2) × 2 | O1–Li1/Os1–O2 | 174.95(17) × 2 |
| Li1/Os1–O2 | 1.924(19) × 2 | | |
| Li2/Os2–O1 | 1.97(13) × 2 | O1–Li2/Os2–O2 | 172.2(3) × 2 |
| Li2/Os2–O2 | 2.069(7) × 2 | O2–Li2/Os2–O2 | 179.7(3) |
| Li2/Os2–O2 | 2.26(14) × 2 | | |
| Li3/Os3–O1 | 2.08(9) × 2 | O1–Li3/Os3–O1 | 179.2(3) |
| Li3/Os3–O1 | 2.214(8) × 2 | O1–Li3/Os3–O2 | 176.7(2) × 2 |
| Li3/Os3-O2 | 2.03(8) × 2 | | |
| Li4/Os4–O1 | 2.43(4) × 2 | O1–Li4/Os4–O2 | 167.7(3) × 2 |
| Li4/Os4–O2 | 1.95(4) × 2 | O2–Li4/Os4–O2 | 151.9(3) |
| Li4/Os4–O2 | 2.162(14) × 2 | | |

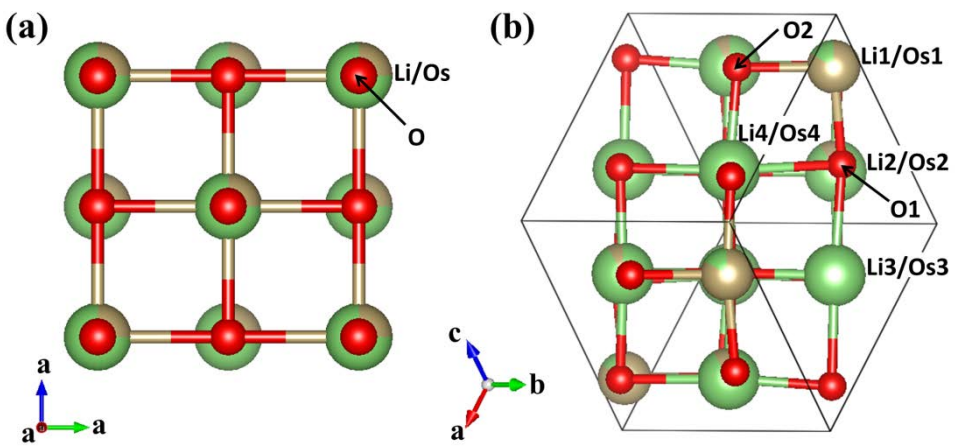


Fig. 3. Crystal structures of (a) cubic $Li_3OsO_4$, and (b) monoclinic $Li_3OsO_4$. The green, brown, and red solid spheres represent Li, Os, and O, respectively.

The crystal structure of cubic $Li_3OsO_4$ is an ideal rocksalt structure as shown in Fig. 3, where the cation sites are occupied by both, Li and Os. The crystal structure of monoclinic $Li_3OsO_4$ evolves from the rocksalt structure by cation ordering. The cation ordering gives rise to a monoclinic supercell. The O–Li/Os–O bond angles deviate from the ideal 180º value and range from 151.9 to 179.7° (see Table 2).

Relevant bond lengths as obtained from the 353 K neutron diffraction data are summarized in Table 2. For the Os-dominant octahedra, the average bond length for Li1/Os1–O is 1.97 Å, which is comparable to the values reported for $Os^{5+}$ oxides, such as 1.96 Å for $Ca_2FeOsO_6$ [39], $Sr_2ScOsO_6$ [40], $La_2NaOsO_6$ [41], or 1.97 Å for $Pr_2NaOsO_6$ [41]. This indicates that Os atoms in the monoclinic title compound are basically pentavalent. However, due to the nonstoichiometricity according to the composition $Li_{3.045}{}^{+1}Os_{0.955}{}^{+5.19}O_4$ as obtained from refinement, a small share of $Os^{6+}$ might be present in the sample. For the Li-dominant octahedra, the average bond lengths are 2.10, 2.11, and 2.18 Å for Li2/Os2–O, Li3/Os3–O, and Li4/Os4–O, respectively, which are in a reasonable range, 2.10–2.21 Å, for $Li^{+1}$-centered octahedra [35–37]. However, it should be noted that the Li4/Os4-centered octahdedra shows exceptional high degree of distortion as the bond angles O–Li4/Os4–O are 151.9(3)º and 167.7(3)º deviating from 180º. The corresponding bond angles for the other octahedral sites in $Li_3OsO_4$ are in the range of 172.2º to 179.7º which are close to 180º. For isostructural compounds $Li_3RuO_4$ [37] and $Li_3SbO_4$ [36], the corresponding band angles are larger than 171.88(12)º and 170.19(15)º, respectively.

The crystal structure of monoclinic $Li_3OsO_4$, projected along *c* and *a* axis, is shown in Fig. 4, where the Os-dominant sites are drawn as octahedra. The Os-dominant

octahedra are not isolated from each other but form edge-sharing zigzag chains. The distance for the nearest Os ions are $d_{Os\text{-}Os}$ = 2.97(2) Å inside the chains.

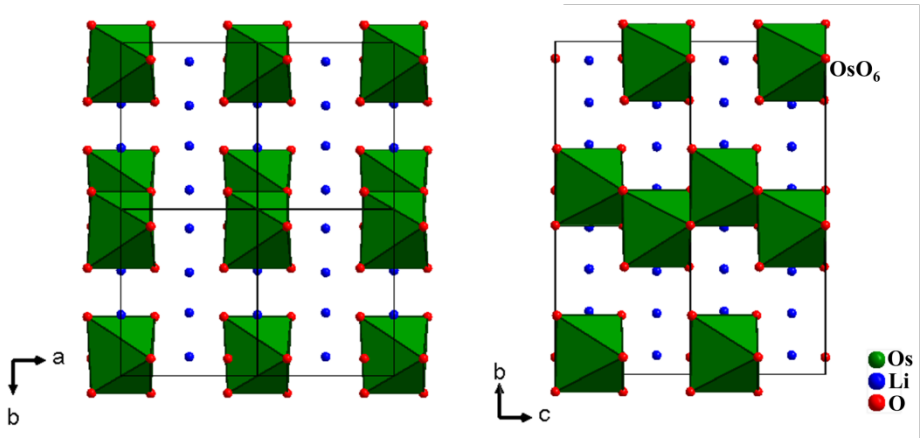


Fig. 4. Projections of the crystal structure of monoclinic $Li_3OsO_4$, view directions [001] (left) and [100] (right).

In our neutron diffraction study, we have investigated the structural changes of monoclinic $Li_3OsO_4$ in the temperature range from 2 to 352 K. In Fig. 5 the thermal variation is shown for the reflection groups –202/121 and –321/–123/040/202, where the changes are strongly pronounced. From 352 K down to 130 K the intensities and positions of the reflection groups –202/121 and –321/–123/040/202 show a notable continuous change, while below 130 K the structure develops into a well stabilized low-temperature state down to 2 K. On the other hand, no broadening could be observed for the reflections 100 and 010 (see Fig. 6). Further, the position of 100 remains practically unchanged suggesting that the lattice parameter *a* does not change. The 010 only shows a slight change of its 2θ position to higher angles indicating a decrease of the respective lattice parameter *b* from 5.890(1) to 5.850(1) Å. Therefore strong structural changes have to be ascribed to the change of the lattice parameter *c* and the monoclinic angle *β*. However, it

was not possible to get a successful profile refinement for the data set collected at 2 K. Furthermore from our analysis it was not possible to find a lower symmetric space group. At this point, we only can assume that a strain occurs along a particular direction, and increases continuously from 352 down to about 130 K. The cause of these distortions may be ascribed to the fact that $Li^+$ ions may change their positions as a function of the temperature. Below 130 K the structure finally reaches a well stabilized state. Due to the anisotropic peak broadening we only could obtain a satisfactory profile fit of the data set collected at 352 K.

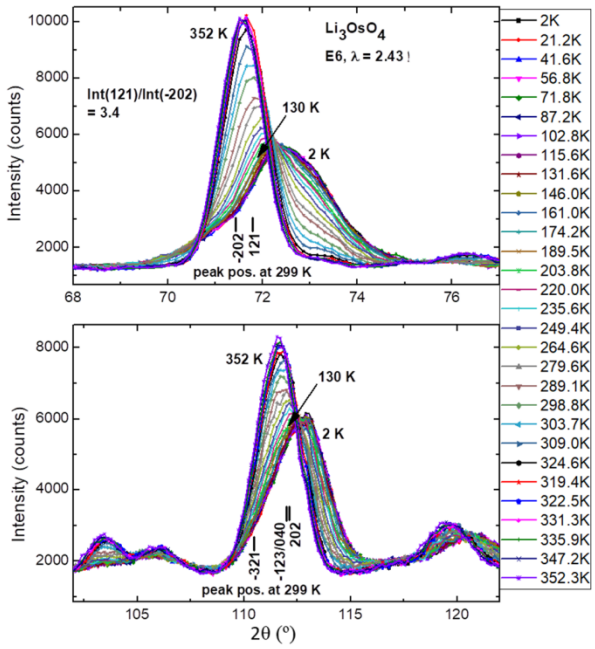


Fig. 5. Temperature dependence of the shifts of particular Bragg reflections of monoclinic $Li_3OsO_4$, see text.

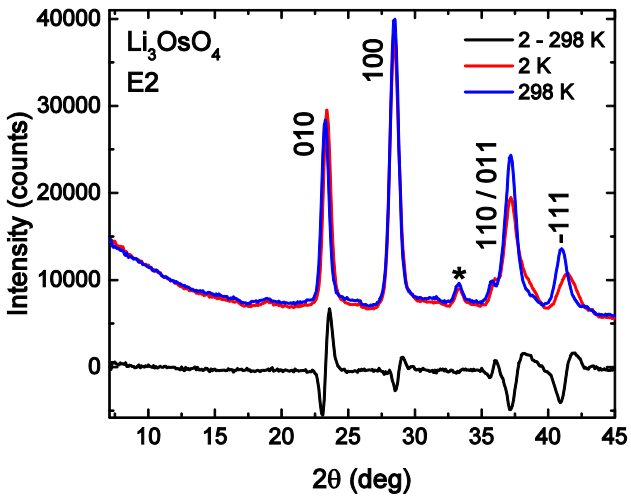


Fig. 6. Neutron powder patterns of monoclinic $Li_3OsO_4$ collected at 2 K and 298 K on the instrument E2. The sample contains a minor amount $Li_2CO_3$, where the reflection observed at 33.3° is marked with an asterisk. The difference of patterns (black) is shown in the lower part of the pattern.

**Electric resistivity**. Both the cubic and monoclinic $Li_3OsO_4$ samples show semiconducting behavior (see Fig. 7): the electrical resistivity (ρ) increases when the temperatures decrease. At 400 K, monoclinic $Li_3OsO_4$ shows a much higher resistivity of ρ = 9062 Ωcm than cubic $Li_3OsO_4$ (7 Ωcm). The ln(ρ) vs. $T^{-1}$ data of monoclinic $Li_3OsO_4$ show linear behavior and the estimated activation energy amounts to ≈ 0.5 eV. In contrast, for cubic $Li_3OsO_4$ the ln(ρ) data show a roughly linear behavior on the $T^{-1/4}$ scale, which is in accordance with a three dimensional variable range hopping transport model.

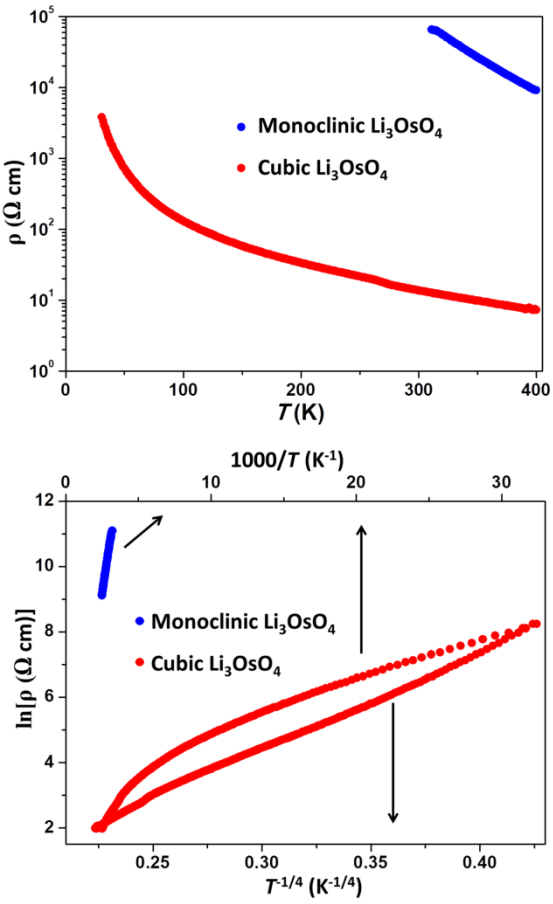


Fig. 7. Temperature dependence of the resistivities of cubic $Li_3OsO_4$ and monoclinic $Li_3OsO_4$. The bottom panel shows the corresponding data with $T^{-1}$ and $T^{-1/4}$ scale.

**Magnetism.** The temperature dependent magnetic susceptibilities (χ) for both, cubic and monoclinic $Li_3OsO_4$, are shown in Figure 8. Cubic $Li_3OsO_4$ displays no sign for magnetic order down to 2 K. The $\chi(T)$ data of monoclinic $Li_3OsO_4$ show an anomaly around 310 K, indicating possible antiferromagnetic transition. The $\chi^{-1}(T)$ data of the cubic $Li_3OsO_4$ is not linear and do not obey the Curie-Weiss law. Attempts to correct the data by considering a temperature independent term $\chi_0$ have failed. For example, when assuming $\chi_0 = 4.5 \times 10^{-4}$ emu mol$^{-1}$, a value comparable to those in other 5*d* oxides $AOsO_3$ [42] and $A_2ScIrO_6$ [43], the corresponding $(\chi - \chi_0)^{-1}(T)$ data neither obey the Curie-Weiss Law (see the inset in Fig. 8).

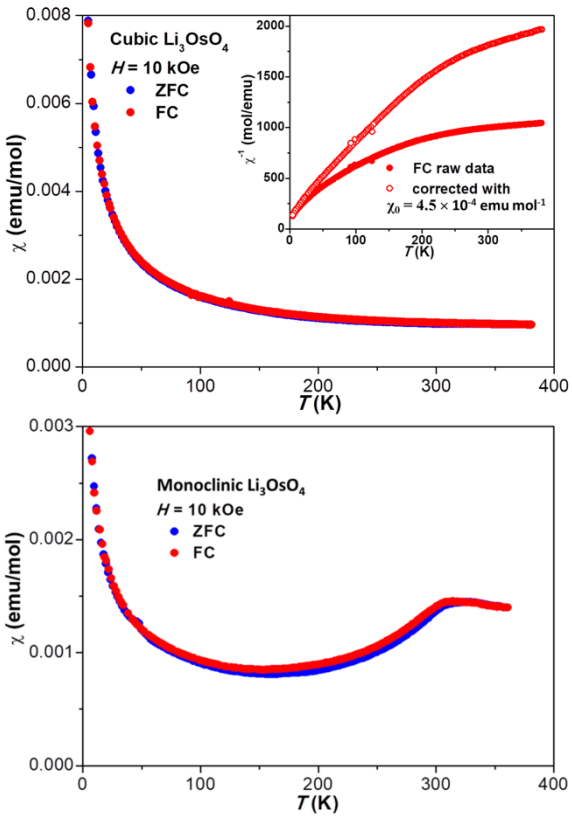


Fig. 8. Temperature dependence of the magnetic susceptibility of cubic $Li_3OsO_4$ (top) and monoclinic $Li_3OsO_4$ (bottom). For cubic $Li_3OsO_4$ data, a 2.0% of mass for KCl and Os was subtracted. The inset shows the corresponding $\chi^{-1}$ vs. T, and $(\chi - \chi_0)^{-1}$ vs. T data, where $\chi_0 = 4.5 \times 10^{-4}$ emu mol$^{-1}$.

To understand the nature of the magnetic anomaly at 310 K, a neutron diffraction study was carried out. However, no magnetic diffraction peak was observed down to 2 K (Fig. 6), indicating that the transition seen in the $\chi(T)$ data of monoclinic $Li_3OsO_4$ may be not related to a long range magnetic order. One possible interpretation of the data is that the anomaly at 310 K corresponds to on-set of short-range antiferromagnetic ordering within the individual Os-chains. Compared with analogous $Li_3RuO_4$, which shows 3-dimensional magnetic ordering below 40 K [44], the $Li_3OsO_4$ samples feature a much higher degree of anti-site disorder between Li and Os (as discussed in the crystal structure

part) [37]. In a theoretical study by Son et al., the anti-site defects in $Li_3RuO_4$ were found to damage the inter-chain antiferromagnetic coupling [45]. Thus, the considerable anti-site disorder in $Li_3OsO_4$ may hinder the formation of long-range antiferromagnetic ordering as well. Future studies, such as muon spin relaxation, may be useful to investigate in detail the formation of short- and long-range order in monoclinic $Li_3OsO_4$.

## Conclusions

Rocksalt-type $Li_3OsO_4$ variants with disordered and ordered arrangements of Li and Os were synthesized. The disordered phase crystallizes in the ideal rocksalt structure with cubic space group $Fm\bar{3}m$. The ordered phase is isostructural to the $Na_3BiO_4$-type structure ($P2/c$). Analyses of X-ray and neutron diffraction data of monoclinic $Li_3OsO_4$ indicate that there is considerable anti-site disorder of Li and Os and that the sample is nonstoichiometric [$Li_{3.045(5)}Os_{0.955(5)}O_4$]. In monoclinic $Li_3OsO_4$, the octahedra predominantly occupied by Os are not isolated from each other but form edge-sharing zigzag chains. Both, cubic $Li_3OsO_4$ and monoclinic $Li_3OsO_4$, are electrically semiconducting. Cubic $Li_3OsO_4$ did not show any sign of magnetic order down to 2 K. Monoclinic $Li_3OsO_4$ displays an anomaly at 310 K in the $\chi(T)$ data. However, the neutron diffraction study indicated that there is no long-rang magnetic order. The anomaly at 310 K may be caused by short-range antiferromagnetic ordering within the individual Os chains.

## Acknowledgment

The work in Dresden was partially supported by the Deutsche Forschungsgemeinschaft through SFB 1143. We thank H. Borrmann in MPI-CPFS for performing X-ray diffraction measurements.

## References


1. K. Mizushima, P. C. Jones, P. J. Wiseman, J. B. Goodenough, $Li_xCoO_2$ ($0 < x \leq 1$): A new cathode material for batteries of high energy density, Mater. Res. Bull. 15 (1980) 783–789.
2. J. B. Goodenough, Y. Kim, Challenges for rechargeable Li batteries, Chem. Mater. 22 (2010) 257–603.
3. L. A. de Picciotto, M. M. Thackeray, W. I. F. David, P. G. Bruce, J. B. Goodenough, Structural characterization of delithiated $LiVO_2$, Mater. Res. Bull. 19 (1984) 1497–1506.
4. A.D. Robertson, P. G. Bruce, Mechanism of electrochemical activity in $Li_2MnO_3$, Chem. Mater. 15 (2003) 1984–1992.
5. M.G. S. R. Thoma, W. I. F. David, J. B. Goodenough, Synthesis and structural characterization of the normal spinel $Li[Ni_2]O_4$, Mater. Res. Bull. 20 (1985) 1137–1146.
6. S. Yamada, M. Fujiwara, M. Kanada, Synthesis and properties of $LiNiO_2$ as cathode material for secondary batteries, Journal of Power sources 54 (1995) 209–213.
7. M. Nakajima, N. Yabuuchi, Lithium-excess cation-disordered rocksalt-type oxide with nanoscale phase segregation: $Li_{1.25}Nb_{0.25}V_{0.5}O_2$, Chem. Mater. 29 (2017) 6927–6935.
8. N. Yabuuchi, M. Nakayama, M. Takeuchi, S. Komaba, Y. Hashimoto, T. Mukai, H. Shiiba, K. Sato, Y. Kobayashi, A. Nakao, M. Yonemura, K. Yamanaka, K. Mitsuhara, T. Ohta, Origin of stabilization and destabilization in solid-state redox reaction of oxide ions for rechargeable lithium batteries. Nat. Commun. 7 (2016) 13814.

9. J. C. Anderson, M. Schieber, Ordered-disorder transitions in heat-treated rock-salt lithium ferrite. J. Phys. Chem. Solids 25 (1964) 961–968.
10. G. Blasse, On the structure of some compounds $Li_3Me^{5+}O_4$ and some other mixed metal oxides containing lithium. Z. anorg. Allg. Chem. 331 (1964) 44–50.
11. S. L. Jibble, I. D. Fawcett, A. C. Hannon, Structure of two disordered molybdates, $Li_2Mo(IV)O_3$ and $Li_4Mo(IV)_3O_8$, from total neutron scattering. Acta Cryst. B53 (1997) 604–612.
12. K. Hirota, Y. Nakazawa, M. Ishikawa, Magnetic properties of the S = 1/2 antiferromagnetic triangular lattice $LiNiO_2$, J. Phys.: Condens. Matter 3 (1991) 4721–4730.
13. J.N. Reimers, J.R. Dahn, J.E. Greedan, C.V. Stager, G. Liu, I. Davidson, U. von Sacken, Spin glass behavior in the frustrated antiferromagnetic $LiNiO_2$, J. Solid State Chem. 102 (1993) 542–552.
14. S.J. Clarke, A.J. Fowdes, A. Harrison, R.M. Ibberson, M.J. Rossiensky, Synthesis, structure, and magnetic properties of $NaTiO_2$, Chem. Mater. 10 (1998) 372–384.
15. Y. Miura, Y. Yasui, T. Moyoshi, M. Sato, K. Kakurai, Magnetic excitations of spin-gap system $Na_3Cu_2SbO_6$ with distorted honeycomb structure, J. Phys. Soc. Jpn. 77 (2008) 104709.
16. L. Viciu, Q. Huang, E. Morosan, H.W. Zandbergen, N.I. Greenbaum, T. McQueen, R.J. Cava, Structure and basic magnetic properties of the honeycomb lattice compounds $Na_2Co_2TeO_6$ and $Na_3Co_2SbO_6$, J. Solid State Chem. 180 (2007) 1060–1067.
17. W. Witczak-Krempa, G. Chen, Y. B. Kim, L. Balents, Correlated quantum phenomena in the strong spin-orbit regime. *Annu. Rev. Condens. Matter Phys.* **2014**, *5*, 57–82.

18. T. Takayama, A. Kato, R. Dinnebier, J. Nuss, H. Kono, L.S.I. Veiga, G. Fabbris, D. Haskel, H. Takagi, Hyperhoneycomb Iridate β-$Li_2IrO_3$ as a platform for kitaev magnetism. Phys. Rev. Lett. 114 (2015) 077202.
19. M. Majumder, R. S. Manna, G. Simutis, J. C. Orain, T. Dey, F. Freund, A. Jesche, R. Khasanov, P. K. Biswas, E. Bykova, N. Dubrovinskaia, L. S. Dubrovinsky, R. Yadav, L. Hozoi, S. Nishimoto, A. A. Tsirlin, P. Gegenwart, Breakdown of magnetic order in the pressurized kitaev iridate β-$Li_2IrO_3$.Phys. Rev. Lett. 120 (2018) 237202.
20. A. Ruiz, A. Frano, N. P. Breznay, I. Kimchi, T. Helm, I. Oswald, J. Y. Chan, R. J. Birgeneau, Z. Islam, J. G. Analytis, Correlated states in β-$Li_2IrO_3$ driven by applied magnetic fields. Nat. Commun. 8 (2017) 961.
21. P.-H. T. Nguyen, M. C. Kemei, M. S. Tan, S. Derakhshan, Synthesis, crystal structure and magnetic properties of the two polymorphs of novel $S$ = 1 osmate; $Li_4MgOsO_6$. J. Solid State Chem. 242 (2016) 155–160.
22. S. Derakhshan, J. E. Greedan, L. M .D. Cranswick, Long-range antiferromagnetic ordering in the S = 1/2 ordered rocksalt oxide $Li_5OsO_6$: comparison with the isoelectronic and isostructural spin glass $Li_4MgReO_6$. Phys. Rev. B 77 (2008) 014408.
23. Y. G. Shi, Y. F. Guo, S. Yu, M. Arai, A. A. Belik, A. Sato, K. Yamaura, E. Takayama-Muromachi, H. F. Tian, H. X. Yang, J. Q. Li, T. Varga, J. F. Mitchell, S. Okamoto, Continuous metal-insulator transition of the antiferromagnetic perovskite $NaOsO_3$. *Phys. Rev. B* **2009**, *80*, 161104(R).
24. S. Calder, V. O. Garlea, D. F. McMorrow, M. D. Lumsden, M. B. Stone, J. C. Lang, J.-W. Kim, J. A. Schlueter, Y. G. Shi, K. Yamaura, Y. S. Sun, Y. Tsujimoto, A. D. Christianson, Magnetically driven metal-insulator transition in $NaOsO_3$. *Phys. Rev. Lett*. **2012**, *108*, 257209.

25. Y. Shi, Y. F. Guo, X. Wang, A. J. Princep, D. Khalyavin, P. Manuel, Y. Michiue, A. Sato, K. Tsuda, S. Yu, M. Arai, Y. Shirako, M. Akaogi, N. Wang, K. Yamaura, A. T. Boothroyd, A ferroelectric-like structural transition in a metal. *Nat. Mater*. **2013**, *12*, 1024–1027.

26. H. Glaser, PhD Thesis, Technische Hochschule, Karlsruhe, 1961

27. G. Brauer, Handbuch der Präparativen Anorganischen Chemie, Ferdinand Elke Verlag, Stuttgart, Germany 1978, 950–951.

28. F. Izumi, K. Momma, Three-dimensional visualization in powder diffraction, Solid State Phenomena 130 (2007) 15–20.

29. K. Momma, F. Izumi, VESTA: a three-dimensional visualization system for electronic and structural analysis, J. Appl. Crystallogr. 41 (2008) 653–658.

30. J. Rodríguez-Carvajal J, *Physica B* **192**, 55–69 (1993).

31. V. F. Sears, in *International Tables for Crystallography* edited by A. J. C. Wilson (Dordrecht/Boston/London: Kluwer Academic Publishers, 1995) Vol. C, p. 383.

32. D. Mikhailova, A. Voss, S. Oswald, A. A. Tsirlin, M. Schmidt, A. Senyshyn, J. Eckert, H. Ehrenberg, Lithium Insertion into $Li_2MoO_4$: Reversible Formation of $(Li_3Mo)O_4$ with a Disordered Rock-Salt Structure, Chem. Mater. 27 (2015) 4485–4492.

33. J. C. Grenier, C. Martin, A. Durif, Etude cristallographique des orthoniobates et orthotantalates de lithium, Bull. Soc. fr. minéral. cristallogr. 87 (1964) 316–320.

34. B. Schwedes and R. Hoppe, Über Oxobismutate. Zur Kenntnis von $Na_3BiO_4$ und $Na_3SbO_4$, Z. anorg. allg. Chem. 393 (1972) 136–148.

35. S. Bernes, S. T. Tovar, M. A. Castellanos R, A comparison of the X-ray single-crystal structure of $Li_3SbO_4$ with the Rietveld refinement. Acta Cryst. C57 (2001) 883–884.

36. J. M. S. Skakle, M. A. Castellanos, S. T. Tovar, S. M. Fray, A. R. West, The crystal structure of $Li_3SbO_4$. J. Mater. Chem. 6 (1996) 1939–1942.
37. A. Alexander, P. D. Battle, J. C. Burley, D. J. Gallon, C. P. Grey, S. H. Kim, Structural and magnetic properties of $Li_3RuO_4$. J. Mater. Chem. 13 (2003) 2612–2616.
38. H. Effenberger and J. Zeemann, Verfeinerung der Kristallstruktur des Lithiumkabonates, $Li_2CO_3$, Z. Kristallogr. 150 (1979) 133–138.
39. H. L. Feng, M. Arai, Y. Matsushita, Y. Tsujimoto, Y. Guo, C. I. Sathish, X. Wang, Y.-H. Yuan, M. Tanaka, K. Yamaura, High-temperature ferrimagnetism driven by lattice distortion in double perovskite $Ca_2FeOsO_6$, J. Am. Chem. Soc. 136 (2014) 3326–3329.
40. A. Taylor, R. Morrow, D. Singh, S. Calder, M. Lumsden, P. Woodward, A. Christianson, Magnetic order and electronic structure of the $5d^3$ double perovskite $Sr_2ScOsO_6$, Phys. Rev. B 91 (2015) 100406.
41. W. R. Gemmill, M. D. Smith, R. Prozorov, H.-C. zur Loye, Crystal growth and magnetic properties of lanthanide-containing osmium double perovskite, $Ln_2NaOsO_6$ (Ln = La, Pr, Nd), Inorg. Chem. 44 (2005) 2639–2646.
42. Y. Shi, Y. Guo, Y. Shirako, W. Yi, X. Wang, A. A. Belik, Y. Matsushita, H. L. Feng, Y. Tsujimoto, M. Arai, N. Wang, M. Akaogi, K. Yamaura, High-Pressure Synthesis of 5d Cubic Perovskite $BaOsO_3$ at 17 GPa: Ferromagnetic Evolution over 3d to 5d Series, J. Am. Chem. Soc. 135 (2013) 16507–16516.
43. P. Kayser, B. J. Kennedy, B. Ranjbar, Spin-orbit coupling controlled ground state in the Ir(V) perovskites $A_2ScIrO_6$ (A = Ba or Sr), Inorg. Chem. 56 (2017) 2204–2209.
44. P. Manuel, D. T. Adroja, P.-A. Lindgard, A. D. Hillier, P. D. Battle, W.-J. Son, M.-H. Whangbo, Neutron scattering and μSR investigations of quasi-one-dimensional magnetism in the spin = 3/2 compound $Li_3RuO_4$, Phys. Rev. B 84 (2011) 174430.
45. W. –J. Son, P. Manuel, D. Adroja, M.-H. Whangbo, Density functional analysis of the

magnetic structure of $Li_3RuO_4$: Importance of the Ru-O···O-Ru spin-exchange interactions and substitutional Ru defects at the Li sites. Inorg. Chem. 50 (2011) 9400–9405.